Green preparation of silk nanofiber membranes from natural silkworms for effective dye/salt fractionation

Bofan Li[1*], Casandra Hui Teng Chai[2], Xue Qi Koh[2], Karen Yuanting Tang[1], Chui Yu Chan[2], Jerry Zhi Xiong Heng[2], Sheng Wang[1], Nannan Wang[1], Enyi Ye[1,2*], Zibiao Li[1,2,3*]

[1] Institute of Sustainability for Chemicals, Energy and Environment (ISCE[2]), Agency for Science, Technology, and Research (A*STAR), 1 Pesek Road, Jurong Island, Singapore 627833, Republic of Singapore.

[2] Institute of Materials Research and Engineering (IMRE), Agency for Science, Technology, and Research (A*STAR), 2 Fusionopolis Way, Innovis #08-03, Singapore 138634, Republic of Singapore.

[3] Department of Materials Science and Engineering, National University of Singapore, Singapore 117576, Republic of Singapore.

*Corresponding authors. E-mail: li_bofan@isce2.a-star.edu.sg (B. Li); yeey@imre.a-star.edu.sg (E. Ye); lizb@imre.a-star.edu.sg (Z. Li)

Abstract

While membranes are widely used in sustainable separations, they are mostly made from petroleum-based polymers and toxic solvents, which are not only harmful to the environment, but also pose a major risk to the safety and health of people. Aiming to enhance the sustainability of fabricating membranes, a biobased silk nanofiber (SNF) membrane is uniquely developed from natural silkworms using green solvents and pressure-assisted deposition method for dye/salt fractionation. One key feature is the replacement of traditional toxic solvents used for SNF extraction to a green solvent, deep eutectic solvent (DES) which is utilized and recycled for SNF preparation. The use of DES can effectively weaken the bonding to disintegrate the silk fibers into microfibrils without destroying the inherent properties of silk fibers. Various SNF loadings were explored to investigate the self-assembling of SNF and optimize the separation performance. The optimized SNF membrane exhibits a high separation factor of 110.7 and remarkable stability in continuously separating NaCl and rose bengal for 100 hours. As compared to the conventional membranes for dye/salt fractionation, the newly developed biobased SNF membrane significantly reduces the environmental hazard by incorporating renewable polymers and green solvents, offering a promising pathway towards the establishment of a sustainable membrane industry.

Key words: Biobased polymers; green solvents; silk nanofibers; deep eutectic solvents; dye/salt fractionation

1. Introduction

Sustainable manufacturing is increasingly popular in companies due to its green strategies, cost reduction in operations and minimized environmental impact [1-3]. Treating industrial wastewater and recycling the valuable components are crucial in the establishment of circular economy in industrial processes [4]. One major wastewater contributor is the textile industry. In China, a daily average of 2 million cubic meter of dye wastewater is discharged which would mean approximately 100,000 tons of dyes and 10 million tons of inorganic salts can be recycled yearly [5]. High concentration of salts are found in wastewater as they are intentionally added to enhance the adhesion of dyes [6]. With membrane technology as an emerging technique, it is effective in tackling the above issues due to its sustainability and efficiency. Its added advantages include low energy consumption, compact and modular design and simple operation [7-9]. Nanofiltration membranes are capable in effectively retain small organic solutes and divalent salts with pore sizes of 0.5-2 nm. However, a significant drawback arises, given that nanofiltration membranes rely on materials derived from fossil resources, such as polysulfone, polyether sulfone, and polyacrylonitrile, for the fractionation of dye and salt mixtures [10-12]. Furthermore, the membrane wastes are typically disposed via landfill or incineration, thus, adding on to the existing soil pollution and greenhouse gases [13-17].

In accordance with the twelve principles of green chemistry, a blueprint of sustainable circular membrane industry is devised, where renewable polymers and green solvents are used in the fabrication of the membranes [13, 14, 18-21]. Currently, renewable polymers are mostly biobased polymers derived from either bacterial fermentation or vegetables and animals. For example, lignin and cellulose are extracted from plant fibers of wood, cotton, straw and bamboo. Sericin and fibroin are sourced from silk fibers, while chitosan is obtained from chitin, which exists in the outer shells of crustaceans. These materials possess high hydrophilicity,

biocompatibility and biodegradability, coupled with low toxicity, carbon footprint and environmental impact [22-24]. However, a dilemma persists concerning the trade-off between the processability and stability of biobased polymers, imposing limitations on their applicability in membranes. Furthermore, with its limitation to produce biobased polymers at production scale and their elevated cost diminishes their economic attractiveness compared to petroleum-based materials [13, 22].

Natural silk fiber is a natural protein fiber that is commonly extracted from the Bombyx mori silkworm cocoon and it is largely used in the textiles for centuries. It consists of two main proteins: 70-80% fibroin and 20-30% sericin, where the fibroin is the structural component and the sericin is the adhesive that holds the fibers together [25]. Silk fibroin is known to be one of the strongest elastomeric biomaterials with remarkable strength, durability and lightweight properties. It is commonly extracted from natural silkworms through degumming and dissolution processes [26]. At present, a variety of acid solvents or aqueous solution of inorganic salts, such as 1,1,1,3,3,3-Hexafluoro-2-propanol (HFIP), N-methyl morpholine N-oxide (NMMO), and hexafluoroacetone hydrate, have been employed to generate silk fibroin. However, most of them are toxic and may destroy the structural hierarchy of silk fibers [27, 28].

To improve the sustainability of membrane fabrication process and reduce the utilization of petroleum-based polymers, herein, we propose a green and facile strategy to prepare a silk nanofiber (SNF) composite membrane for dye/salt fractionation to treat textile wastewater. SNF was first extracted from natural silkworms using a deep eutectic solvent (DES), which is a type of ionic liquid containing large nonsymmetric ions that have low lattice energy and low melting point [29]. It is often regarded as a green solvent due to its low vapor pressure,

nonflammability, ease of preparation and good recyclability. Next, SNF was self-assembled onto a cellulose acetate substrate via a pressure-assisted deposition method. Various SNF loadings on the membrane were investigated and the developed membranes were found to exhibit excellent separation performance and stability in fractionating dye/salt mixture for resource recovery in textile industries. Moreover, it is envisioned that the developed SNF composite membrane that utilizes biobased polymers and green solvents can reduce environmental impact, thus contributing to the advancement of sustainable membrane industry.

2. Experimental

2.1 Materials

Choline chloride, sodium carbonate and oxalic acid were purchased from Sigma-Aldrich. B. mori cocoons were purchased from Nanoflux Pte Ltd and were used after removal of the sericin proteins by boiling in an aqueous solution of sodium carbonate. The cellulose acetate membrane substrate (pore size: 0.22 μm) was purchased from Hangzhou Special Paper Industry Co. Ltd. Dopamine hydrochloride (Sigma-Aldrich) was employed to increase the adhesion between silk nanofibers and the substrate. All chemicals were used as received without further purification. In all washing steps, deionized (DI) water (18.2 MΩ) was used.

2.2 Preparation of silk nanofibers

B.mori cocoons were degummed in a boiling solution of 0.5 wt% sodium carbonate for 30min. The degummed silk fibers were washed with distilled water and left to dry overnight. The DES was prepared by dissolving equimolar choline chloride (ChCl) and oxalic acid at 80 °C to form a transparent solution. 1g of silk fibers were cut into small pieces and added into the DES. The as-prepared dispersion was mixed and heated to 110°C for 24 h to produce a glue-like dispersion. The produced silk nanofibers were removed and washed using filtration to remove

any residue, followed by drying overnight. Silk nanofibers were then re-dispersed in DI water using ultrasonication (Q Sonica, sonicator).

The recycling of DES was conducted by concentrating the diluted DES solution using a rotary evaporator to remove bulk of the water. It was then further heated in a vacuum oven for 24 h at 60 °C to remove any excess water content in the concentrated DES solution. The recycled DES obtained was weighed to determine the DES recovery percentage after pre-treatment.

2.3 Preparation of silk nanofiber composite membranes

Prior to the deposition of silk nanofibers, the cellulose acetate substrate was modified with dopamine to enhance its affinity with silk nanofibers. Dopamine was chosen due to its effective adhesion properties and good biocompatibility. It was expected to aid in the placement of silk nanofibers, thus promoting secure adhesion of the silk nanofibers to the substrate, preventing easy delamination [30, 31]. Initially, 0.2 g of dopamine hydrochloride was dissolved in 100 mL of a 0.01M Tris buffer at pH 8.5. Subsequently, the resulting solution was applied to the upper surface of the substrate at room temperature and left for 1 hour. Following this, the substrate was rinsed with DI water to remove the residues.

The as-prepared silk nanofiber aqueous dispersion was filtered through the dopamine-modified substrate in a dead-end filtration cell at 1 bar by means of a pressure-assisted deposition method. Four types of membranes with different SNF loadings, namely 20.8, 41.6, 83.2 and 124.7 g m^{-2} were prepared to optimize the membranes performance, which are labelled as SNM-5, SNM-10, SNM-20 and SNM-30, respectively. The as-prepared composite membranes were cured at 60 °C for 5 min in an oven to evaporate residual water. This process facilitated the formation of hydrogen bonds between the silk nanofibers, thereby enhancing structural stability and

mitigating the risk of silk nanofiber delamination. The fabricated silk nanofiber composite membranes were then preserved in DI water for further testing.

2.4 Characterizations

The morphologies of silk nanofibers and the composite membrane were observed by field emission scanning electron microscopy (FESEM, JEOL JSM7600F). Silk nanofiber aqueous dispersion was dripped onto a silica wafer and vacuum dried. Membrane samples were freeze-dried and fractured in liquid nitrogen. Both samples were coated with a thin layer of gold using a JEOL JFC-1200 coater for FESEM observation. The silk nanofibers and composite membranes were probed using atomic force microscope (AFM) (Bruker JPK NanoWizard 4XP) under the standard tapping mode (in air), with a scanning rate at 0.5 Hz and scan size of 50 x 50 μm. The average roughness (R_a) and root-mean-square roughness (R_q) were derived from the triplicates average of R_a and R_q values at different areas, respectively. Transmission electron microscopy (TEM, FEI Titan 80/300 Thermo Fischer Scientific) was employed to observe the silk nanofibers at an accelerating voltage of 200 KV. The hydrodynamic diameter and zeta potential of the silk nanofibers were measured by a dynamic light scattering (DLS) (Zetasizer Nano ZS90) under room temperature. The pristine silk nanofibers, degummed silk nanofibers and the silk nanofiber composite membranes were examined using Fourier transform infrared spectroscopy (FTIR, Brucker Vertex 80v) under attenuated total reflectance mode.

2.5 Separation performance for dye/salt fractionation

The pure water permeance (PWP, L m^{-2} h^{-1} bar^{-1}, LMH bar^{-1}) of the membrane was evaluated using dead-end filtration cells with a trans-membrane pressure ΔP (bar) of 1 bar at room temperature. The PWP value was determined using the following equation:

$$PWP = \frac{Q}{A\Delta P} \quad (1)$$

where Q (L h^{-1}) represents the water flux at the permeate side and A (m^2) is the effective filtration area of the membrane. To ensure consistent measurements, each membrane sample was assembled and left to stabilize for 1 h before measurement. For each condition, a minimum of three membrane samples were measured to ensure reliable results and the average results were reported.

The rejections to dyes and inorganic salts were determined by preparing feed solutions containing 50 ppm dyes or 1000 ppm inorganic salts under a trans-membrane pressure of 1 bar with pre-stabilization of 1 h. The concentrations of dye and salt in both feed (C_f) and permeate (C_p) were determined using a UV-Vis spectrophotometer (UV-1800 UV/visible scanning spectrophotometer, Shimadzu) and a conductivity meter (SevenCompact, Mettler-Toledo), respectively. The dye and salt rejections (R, %) were calculated using Eq. (2).

$$R = \left(1 - \frac{C_p}{C_f}\right) \times 100\% \quad (2)$$

The dye/salt fractionation test was conducted using mixed feed solutions containing 50 ppm rose bengal and 1000 ppm NaCl under 1 bar for 100 h. The separation factor of dye and salt was determined using the following equation.

$$Separation\ factor_{\frac{Salt}{Dye}} = \frac{x_{Salt}^{permeant} / x_{Dye}^{permeant}}{x_{Salt}^{feed} / x_{Dye}^{feed}} \quad (3)$$

3. Results and discussion

3.1 Synthesis of SNFs and DES recycling

High purity silk nanofibers were obtained via degumming, DES dissolution and ultrasonication, as illustrated in Fig. 1a. Degumming is an essential step to be carried out as the silk fibers

contains sericin, a natural gum like substance which protects the silk fiber structure. This process is crucial as it breaks the peptide bonds and separate sericin from the fibroin, which is carried out through hydrolytic degumming using sodium carbonate. After the removal of sericin, silk fibroin was dissolved into the prepared DES at 110°C. DES is employed as a green solvent to replace commonly used toxic solvents due to its low toxicity and biodegradability. DES is a type of ionic liquid that can be formed when a hydrogen bond donor and a hydrogen bond acceptor are mixed [29]. With its acidity and significant swelling ability, DES can disrupt the hydrogen bonds and break the fibroin structure to disintegrate the silk fibers into microfibrils [32]. Silk dissolution is a vital step as it directly affects the characteristics of silk fibers which impacts the properties of the resulting silk nanofiber. Silk microfibrils were removed from the DES after dissolution and redispersed in DI water using ultrasonication to obtain silk nanofibers. The water-dispersible synthesized silk nanofibers facilitate the subsequent pressure-assisted deposition on the substrate.

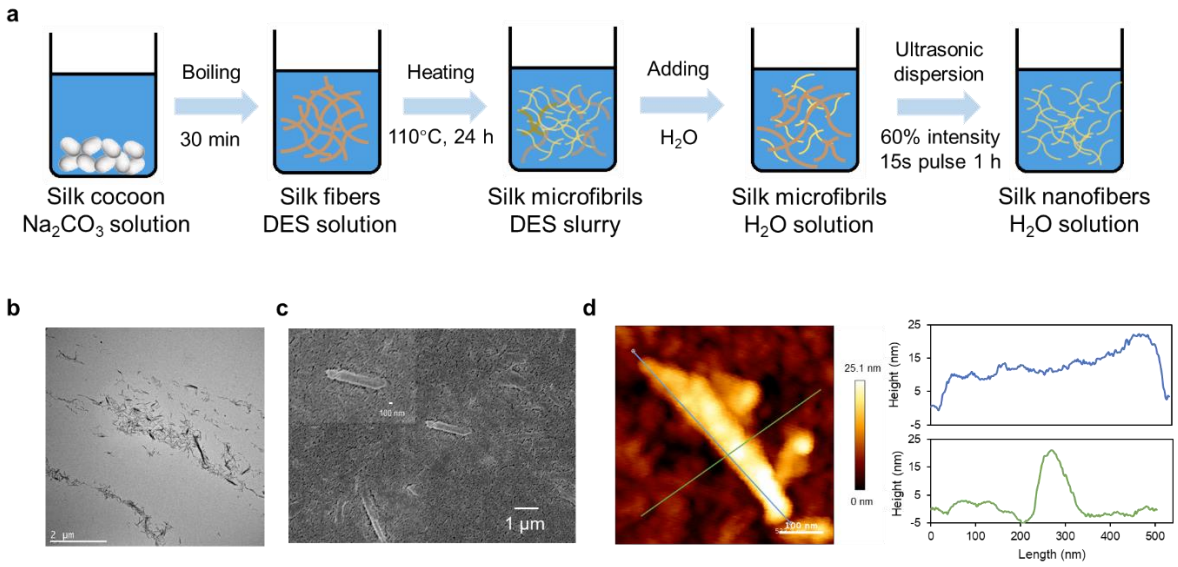

Figure 1 Preparation of SNF and its morphology. a) An illustration of the SNF preparation steps, which comprises degumming, DES dissolution and ultrasonication processes. b) TEM image c) SEM images and d) AFM image and depth profile of the prepared SNFs.

In addition to its low volatility and toxicity, DES can be recycled after silk dissolution and be reused for the next synthesis. As illustrated in Fig. S1, after silk dissolution, the silk fibers are washed with DI water and filtered to remove any excess DES. The diluted DES solution obtained from filtering was then recycled with the use of rotary evaporator and vacuum drying. The recovery percentage of DES is determined to be 78.4% by taking the weight ratio of recovered DES to the initial input for three runs. The good recovery is attributed to the high boiling point and low volatility of DES. This demonstrates DES can serve as an environmentally friendly, economically feasible and sustainable solvent for producing SNFs.

3.2 Characterization of SNFs

The morphology and dimension of synthesized silk nanofibers were characterized by TEM, FESEM, and AFM, as shown in Fig. 1b, c and d, respectively. From TEM image (Fig. 1b), the silk fibers can be seen to be mostly disintegrated into fine nanofibers after the degumming, dissolution and ultrasonication. While a few microfibrils still present, there is no large silk fibers observed, indicating that the DES can effectively disintegrate the silk fibers by weakening or partially destroying the strong hydrogen bonds. In addition, ultrasonication breaks the weak bonding and further disintegrate the fibers into well-dispersed nanofibers. The FESEM image also reveals that the silk nanofibers have been successfully synthesized with widths of a few hundred nanometres and contour lengths of 500-1000 nanometres (Fig. 1c). To detect the topology and quantify the dimension of synthesized nanofibers, AFM is employed by probing the surface of silica wafer with immobilized silk nanofibers. As shown in Fig. 1d, the diameter of the nanofiber is measured to be approximately 20 nm from the depth profile, which aligns well with the diameters of single nanofibers found in natural silks (10-30 nm) [33, 34].

To study the size distribution of the prepared SNFs, dynamic light scattering was employed to measure the hydrodynamic diameter of the SNFs. As shown in Fig. 2a, the size distribution curve of the prepared SNF ranges from 300 nm to 600 nm with a centre at 400 nm. The average hydrodynamic diameter of the prepared SNF is 409 ± 13 nm from three experimental runs. This value is substantially greater than the diameter of SNF determined from AFM, as the contour length of the SNF is much larger than the diameter of SNF. In addition, the hydrodynamic diameter of a particle is defined as the diameter of a sphere that exhibits the translational diffusion speed as the particle of interest. It is generally larger than the size of particle measured from SEM or AFM due to the presence of hydrated water molecules and interactions [35, 36]. Nevertheless, the hydrodynamic diameter can reflect the SNF size distribution and dispersity in water.

The chemistry of silk fibers and possible chemical modification occurred during the synthesis were investigated. The raw cocoon, degummed silk fibers and the obtained SNF were analyzed using FTIR. As shown in Fig. 2b, the strong peaks (1510 and 1618 cm^{-1}) and weak peak (1695 cm^{-1}) located in amide I and II band region are assigned to β-sheets and β-turns of hairpin-folded antiparallel β-sheet structure, respectively [37, 38]. This indicates that the silk fibers mainly consist of stable β-sheet structure with strong hydrogen bonds and van der waals forces. In addition, two minor peaks (1220 cm^{-1} and 1261 cm^{-1}) appear at amide III region, which indicates the existence of coil structure. This demonstrates that the silk fibers mainly contain abundant β-sheet structure with a few random coil conformations, as illustrated in Fig. S2. Moreover, the FTIR spectra of the raw cocoon, degummed silk fiber and as synthesized SNF show identical peaks, implying that there is no chemical modification during the degumming and DES dissolution processes. This confirms that the degumming and DES dissolution processing will not destroy the natural properties of the silk fiber.

Furthermore, the surface charge of the SNFs was characterized by measuring the zeta-potential of SNF aqueous dispersion at different pH conditions. The results show that the zeta-potential of SNF decreases as the pH of SNF dispersion increases, which is due to the complex chemistry of silk fibroin containing various amino acids. The isoelectric point of synthesized SNFs in water is determined to be 4.9, where the surface charge of SNF is neutral. When the pH is below 4.9, the SNFs are positively charged with compacted structures. If the pH increases beyond 4.9, the SNFs become negatively charged, leading to repulsive forces that compel the polypeptide to assume elongated conformations [39, 40]. Therefore, in this study, the pH of as-synthesized SNF dispersion is adjusted to 8 in order to minimize the aggregation of SNFs.

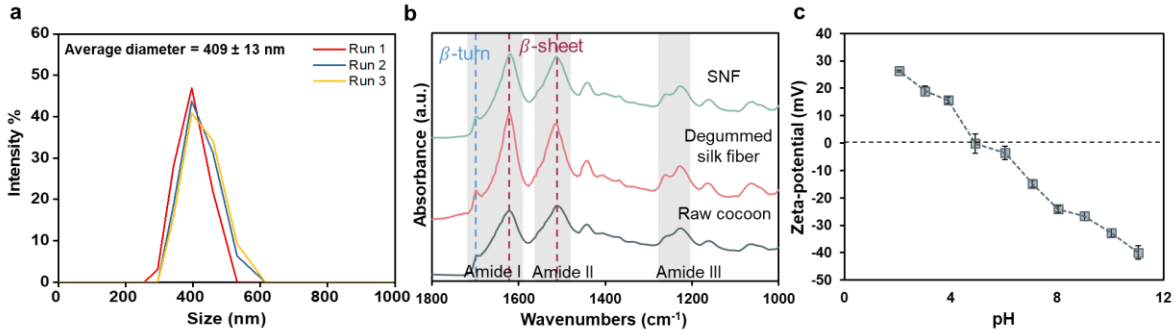

Figure 2 Characterizations of the prepared SNFs. a) Hydrodynamic diameter distribution and the average diameter of SNFs. b) FTIR spectra of raw cocoon, degummed silk fiber and SNF. c) Surface zeta-potential of SNFs at different pH conditions.

3.3 Fabrication and characterization of SNF membranes

The SNF membrane was assembled by depositing the as-prepared aqueous SNF dispersion on a dopamine coated cellulose acetate membrane substrate via a pressure-assisted self-assembling method. This method is straightforward and environmentally friendly, devoid of the inclusion of harmful chemicals. The SNFs can be firmly attached to the substrate due to the good adhesion property of dopamine and possible hydrogen bonding formed between SNF and

cellulose acetate [41, 42]. Different SNF loadings ranging from 20.8 to 124.7 g m^{-2} were deposited onto the substrate and investigated. The membrane morphologies of the prepared SNM-5, SNM-10, SNM-20 and SNM-30 were observed using FESEM and AFM, as shown in Fig. 3a and b, respectively. All the membranes possess uniform surfaces with fibrous structures. The nanofiber morphology can be observed on the surface of membranes, especially on the highly loaded ones. From AFM images, rod-like shape SNFs can be observed on the membrane surface. The membrane surfaces are relatively smooth at low SNF loading but become rough when the SNF loading is increased to 124.7 g m^{-2}. The surface roughness of the prepared membranes is measured at 3 spots and the averaged value is tabulated in Table 1. The root-mean-square (RMS) roughness (R_q) increases slightly from 108.7 to 196.5 nm when the loading increases from 20.8 to 83.2 g m^{-2}, but it dramatically increases to 638 nm when the loading reaches 124.7 g m^{-2}. This is probably due to the self-assembly of SNFs during the deposition process, which is driven by thermodynamics and kinetics as explained in the later section.

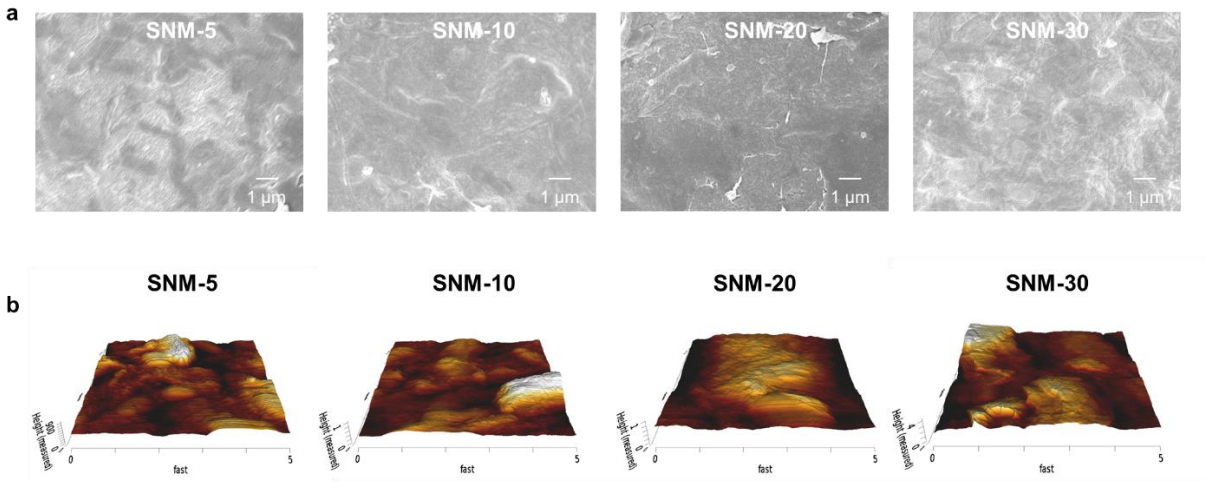

Figure 3 Surface morphologies of fabricated silk nanofiber composite membranes with different SNF loadings. a) FESEM images and b) AFM mappings of SNM-5, SNM-10, SNM-20 and SNM-30 (from left to right).

Table 1 The SNF loading, thickness and surface roughness of prepared SNMs.

Membrane	Silk nanofiber loading (g/m^2)	Selective layer thickness (μm)	Average roughness (Ra)	RMS roughness (Rq)
SNM-5	20.8	4.8 ± 0.4	78.5 ± 3.3	108.7 ±4.5
SNM-10	41.6	12.7 ± 0.3	124.3 ± 3.7	158.6 ±7.2
SNM-20	83.2	37.0 ± 1.0	157.3 ± 6.5	196.5 ± 14.7
SNM-30	124.7	156.1 ± 2.5	517.1 ± 49.3	637.9 ± 16.4

The thickness of the SNF layer is measured from the cross-section images (Fig. S3) and the values are tabulated in Table 1. The thickness of the SNF layer increases with the loading of SNF; however, the thickness increases linearly from 4.8 to 37.0 μm at low SNF loading and it dramatically increases to 156.1 μm when the SNF loading increases further to 124.7 g m^{-2} (Fig. 4a and Table 1). In addition, as observed from the cross-sectional images, SNM-5 and 10 possessed uniform and dense cross-sections. In comparison, the cross-sections of SNM-20 and 30 exhibit a nanofibrous structure, and particularly nanofibrils is observed from the cross-section of SNM-30. The sharp increase of thickness and different morphology can be attributed to the self-assembly and stacking behaviours of SNFs during the deposition process. The self-assembly of SNFs in aqueous dispersion will experience conformation transitions and nanostructure assembly, which is affected by molecular mobility, charge, hydrophilic interactions, and concentration [39]. As aforementioned, the isoelectric point of SNF is determined to be 4.9, so it exhibits negative surface charge in the prepared dispersion for deposition. Previous studies reported that SNFs would first assemble into micelles and aggregate into nanofibrils especially under high concentrations because of the reduced

repulsive forces compared to larger repulsive forces in the case of globule formation [39, 40, 43]. During the deposition process, water will be filtered away slowly, leading to a concentrated SNF dispersion on top of the membrane. In such manner, SNFs tend to assemble into nanofibrils at high loading conditions, resulting in a nanofibrous structure that exhibits increased thickness and surface roughness.

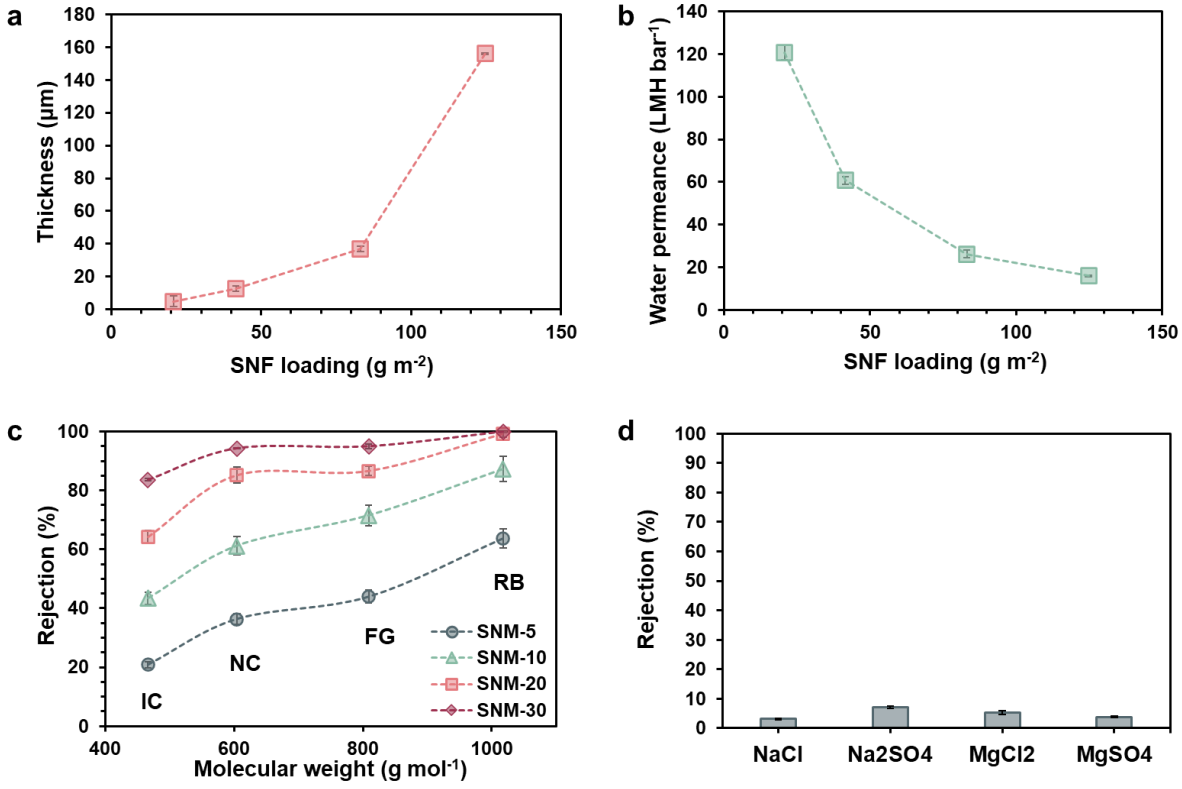

Figure 4 Water permeance and separation performance of the silk nanofiber membrane. a) The relationship between the thickness and SNF loading. b) Water permeances of the silk nanofiber membranes with different SNF loadings. c) Dye rejections of silk nanofiber membranes versus the molecular weights of various dyes. IC: Indigo carmine; NC: New coccine; FG: Fast green FCF; RB: Rose bengal. d) Salt rejections of SNM-20.

3.4 Separation performance for dye/salt fractionation

To investigate the effect of SNF loading on the separation performance of the prepared SNF composite membranes, water permeances and rejections towards various dyes were measured

using SNM-5, 10, 20 and 30. Surprisingly, the SNM-5 exhibits a water permeance of 121 LMH bar^{-1}, which significantly decreases to 26 LMH bar^{-1} when the SNF loading increases to 83.2 g m^{-2} (Fig. 4b). Nevertheless, the rate of decrease in water permeance can be seen to gradually decline when the SNF loading is further increased to 124.7 g m^{-2}. The decrease in water permeance can be ascribed to 1) the increase in the thickness of SNF layer and 2) the densely packed structure of SNF. As aforementioned, the thickness of SNF layer increases linearly at low SNF loading range and rises dramatically when the SNF loading reaches 124.7 g m^{-2}. However, the effect of SNF loading on water permeance deviates from that on membrane thickness, mainly because of the packing structure of SNF on the substrate at different loading conditions. From the cross-sections, SNFs are stacked into a thin and densely packed structure at low SNF loading; as the loading increases, SNFs tend to aggregate and form into a loosely packed nanofibrous structure. Therefore, although the thickness of SNF layer increases significantly at high SNF loading, the water permeance does not decrease significantly because of the loosely packed SNF layer.

To evaluate the separation efficiency of the SNF composite membranes, various dyes, including indigo carmine (IC), new coccine (NC), fast green FCF (FG) and rose bengal (RB), were employed for filtration tests. Table S1 summarizes the properties and molecular structures of the selected dyes. The rejections of SNF composite membranes with different loadings are measured and reported in Fig. 4c. The rejections of the selected four dyes increases with their molecular weights for all the SNF membranes due to the size-exclusion effect. For instance, the rejection towards IC (MW= 466.4 g mol^{-1}) and RB (MW= 1017.6 g mol^{-1}) of SNM-20 is 64% and 99%, respectively. Moreover, the dye rejections increase with the loading of SNFs especially for small molecular dyes, i.e., IC and NC. This is in accordance with the water permeance, as the mass transfer resistance of the membrane increases with the SNF loading.

Among the four prepared membranes, SNM-20 has relatively high water permeance of 26 LMH bar^{-1} and satisfactory rejections towards dyes. Thus, it is selected for further dye/salt fractionation tests. Prior to dye/salt fractionation test, single salt rejection was measured using 1000 ppm of NaCl, Na_2SO_4, $MgCl_2$ and $MgSO_4$ solutions as feed solutions at 1 bar. As shown in Fig. 4d, the salt rejections towards these four salts are very low, ranging from 3 % to 7 %, due to the loose structure and large pore size. The low salt rejection and high dye rejection hold significant promise for treating high-salinity wastewater in the textile industry, where high concentrations of NaCl and Na_2SO_4 are commonly employed to improve dye adhesion to fabrics and maximize dye molecule exhaustion [44, 45].

3.5 Dye/salt fractionation to treat textile wastewater

In order to study the separation performance and stability of prepared SNF composite membrane in treating textile wastewater, a mixed dye/salt solution containing RB and NaCl was continuously filtrated through the membrane for 100 h. Fig. 5a displays the changes in water permeance and rejection towards NaCl and RB over time. The water permeance experiences a slight decrease within the initial 36 hours, possibly attributable to membrane compaction and fouling phenomena. After the compaction and fouling reach saturation, a stable water permeance is achieved during the test. The rejections towards RB and NaCl remain highly consistent throughout the 100-h test, showcasing excellent stability in the context of textile wastewater separation. The water permeance and separation factor, calculated as the ratio of dye to salt concentration in the permeate to that in the feed, are determined and later compared with membranes reported in literature (Fig. 5b and Table S2). The separation factor of SNF composite membrane in separating rose bengal and NaCl is calculated to be 110.7. The separation factor indicates the membrane's efficiency in separating dyes and salts in a mixed solution. A higher separation factor signifies enhanced performance in separating dye and salt

mixtures, an important evaluator that is particularly advantageous for textile wastewater treatment. Compared with the conventional petroleum-based membranes, the newly developed biobased SNF composite membrane exhibits outstanding fractionation capabilities between dyes and salts, surpassing or at least matching the performance of most nanofiltration and ultrafiltration membranes documented in the literature (Fig. 5b).

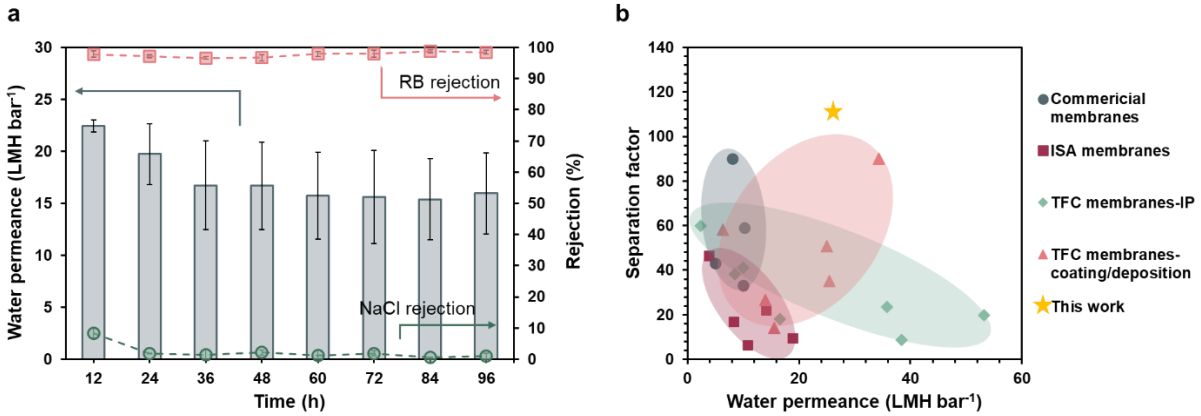

Figure 5 a) Continuous dye/salt fractionation test of SNM-20 in rose bengal/NaCl mixture for 100 h. b) Comparison of separation performance with reported membranes in the literature for dye/salt fractionation.

3.6 Sustainability evaluation

The SNF composite membrane designed in this study employed sustainable materials and green solvents from the macroscale to the nanoscale. Biobased polymers, SNFs and cellulose acetate, were used as the selective layer and support, respectively. The SNFs was extracted by a green DES, which can be recycled and reused for subsequent extraction of SNFs. Cellulose acetate, sourced from the renewable and abundant cellulose, possesses biodegradability, low toxicity, chemical stability, mechanical strength and cost-effectiveness, rendering it a good candidate for membrane substrates. Compatibility between the support and the selective layer was reinforced by depositing an interlayer using an aqueous solution of polydopamine, sourced from mussels, known for its good adhesion and biocompatibility. In addition, no organic

394 solvents were used and only water is employed as the processing medium from silkworms to
395 SNF membranes. This is the first reported biobased membrane that does not consist of any
396 petroleum-based materials for dye/salt fractionation. To compare the sustainability of the
397 newly developed biobased SNF membrane with conventional TFC membranes for dye/salt
398 fractionation, the chemicals in the selective layer were listed and their sustainability were
399 evaluated by the hazard and toxicity as indicated by the Globally Harmonized System of
400 Classification and Labelling of Chemicals. As elaborated in Table S3, TFC membranes
401 fabricated by interfacial polymerization and coating often involves health hazard,
402 environmental hazard or toxic compounds, such as trimesoyl chloride, piperazine and
403 polyethyleneimine. In addition, the fabrication processes usually involve the usage of
404 flammable and volatile solvents, such as hexane and toluene. Our proposed green SNF
405 membrane utilizes natural silkworms and recyclable DES without additional organic solvents
406 and dangerous chemicals, demonstrating the enhanced sustainability over traditional petroleum
407 based and partially green TFC membranes.
408
409 **4. Conclusions**
410 In summary, we have demonstrated a green and simple approach to prepare SNF composite
411 membranes for dye/salt fractionation with excellent and stable separation performance. SNFs
412 are firstly extracted from natural silkworms by substituting traditional toxic solvents with DES,
413 which can be recycled and reused for further extraction process. The as-harvested SNFs
414 preserves the native structures and chemistry, yet they are able to reduce its size to nano scale.
415 The SNF composite membrane is fabricated by self-assembling of SNF via a pressure-assisted
416 self-assembling method. By tuning the SNF loadings, the thickness of SNF selective layer can
417 be varied with different separation performance. Interestingly, the thickness of SNF selective
418 layer increases linearly with the loading when the loading is less than 100 g m^{-2}. However, the

thickness dramatically increases when the loading exceeds due to the formation of loosely packed SNFs nanofibrous structures at high SNF loading, as supported by SEM and water permeance. The optimized SNF composite membrane exhibits a water permeance of 26 LMH bar^{-1} with high rejection of 99% towards rose bengal. Moreover, the developed SNF composite membrane is capable in continuously fractionating dye and salt for 100 h to treat textile wastewater containing high concentrations of dyes and inorganic salts. The membrane demonstrates a stable water permeance with a separation factor of 110.7, which surpasses most ultrafiltration and nanofiltration membranes reported in literature. By utilizing natural resource and green solvent, the SNF composite membrane holds great potential for sustainable water purification and molecular separation to reduce the footprint and minimize the environmental impact.

Acknowledgements

The authors would like to acknowledge the financially supported from the Agency for Science, Technology and Research (A*STAR) under its A*STAR Career Development Fund – Seed Project 2022 (Grant No. C222812032), RIE2025 manufacturing, trade and connectivity (MTC) Young Individual Research Grants (YIRG) (Grant No. M22K3c0103), RIE2025 Manufacturing, Trade and Connectivity (MTC) Programmatic Funding (Grant No. M22K9b0049).

References

[1] Y. Bhatt, K. Ghuman, A. Dhir, Sustainable manufacturing. Bibliometrics and content analysis, J. Clean. Prod., 260 (2020) 120988.

[2] A. Moldavska, T. Welo, The concept of sustainable manufacturing and its definitions: A content-analysis based literature review, J. Clean. Prod., 166 (2017) 744-755.

[3] S.P. Nunes, P.Z. Culfaz-Emecen, G.Z. Ramon, T. Visser, G.H. Koops, W. Jin, M. Ulbricht, Thinking the future of membranes: Perspectives for advanced and new membrane materials and manufacturing processes, J. Membr. Sci., 598 (2020) 117761.

[4] S. Nair K, B. Manu, A. Azhoni, Sustainable treatment of paint industry wastewater: Current techniques and challenges, J. Environ. Manage., 296 (2021) 113105.

[5] J. Chen, Q. Wang, Z. Hua, G. Du, Research and application of biotechnology in textile industries in China, Enzyme Microb. Technol., 40 (2007) 1651-1655.

[6] J. Lin, W. Ye, H. Zeng, H. Yang, J. Shen, S. Darvishmanesh, P. Luis, A. Sotto, B. Van der Bruggen, Fractionation of direct dyes and salts in aqueous solution using loose nanofiltration membranes, J. Membr. Sci., 477 (2015) 183-193.

[7] P. Jin, J. Zheng, Q. Gao, A.K. An, J. Zhu, B. Van der Bruggen, Loose Nanofiltration Membranes for the Treatment of Textile Wastewater: A Review, J. Membr. Sci. Res., 8 (2022).

[8] S. Guo, Y. Wan, X. Chen, J. Luo, Loose nanofiltration membrane custom-tailored for resource recovery, Chem. Eng. J., 409 (2021) 127376.

[9] X. Feng, D. Peng, J. Zhu, Y. Wang, Y. Zhang, Recent advances of loose nanofiltration membranes for dye/salt separation, Sep. Purifi. Technol., 285 (2022) 120228.

[10] A.W. Mohammad, Y.H. Teow, W.L. Ang, Y.T. Chung, D.L. Oatley-Radcliffe, N. Hilal, Nanofiltration membranes review: Recent advances and future prospects, Desalination, 356 (2015) 226-254.

[11] G.M. Shi, Y. Feng, B. Li, H.M. Tham, J.-Y. Lai, T.S. Chung, Recent progress of organic solvent nanofiltration membranes, Prog. Polym. Sci., 123 (2021) 101470.

[12] X.Q. Cheng, Z.X. Wang, X. Jiang, T. Li, C.H. Lau, Z. Guo, J. Ma, L. Shao, Towards sustainable ultrafast molecular-separation membranes: From conventional polymers to emerging materials, Prog. Mater. Sci., 92 (2018) 258-283.

[13] W. Xie, T. Li, A. Tiraferri, E. Drioli, A. Figoli, J.C. Crittenden, B. Liu, Toward the next generation of sustainable membranes from green chemistry principles, ACS Sustainable Chem. Eng., 9 (2021) 50-75.

[14] D. Zou, S.P. Nunes, I.F.J. Vankelecom, A. Figoli, Y.M. Lee, Recent advances in polymer membranes employing non-toxic solvents and materials, Green Chem., 23 (2021) 9815-9843.

[15] B. Li, S. Wang, X.J. Loh, Z. Li, T.S. Chung, Closed-loop recyclable membranes enabled by covalent adaptable networks for water purification, Proc. Natl. Acad. Sci. U.S.A., 120 (2023) e2301009120.

[16] S. Wang, N. Wang, D. Kai, B. Li, J. Wu, J.C.C. Yeo, X. Xu, J. Zhu, X.J. Loh, N. Hadjichristidis, Z. Li, In-situ forming dynamic covalently crosslinked nanofibers with one-pot closed-loop recyclability, Nat. Commun., 14 (2023) 1182.

[17] B. Li, C. Qu, S. Wang, J.C.C. Yeo, N.E.B. Surat'man, X.J. Loh, Z. Li, T.S. Chung, Closed-loop recyclable dynamic covalent crosslinked nanofibrous membranes for efficient oil/water separation, J. Membr. Sci., 693 (2024) 122378.

[18] A. Figoli, T. Marino, S. Simone, E. Di Nicolò, X.M. Li, T. He, S. Tornaghi, E. Drioli, Towards non-toxic solvents for membrane preparation: a review, Green Chem., 16 (2014) 4034-4059.

[19] X. Jiang, W.F. Yong, J. Gao, D.-D. Shao, S.-P. Sun, Understanding the role of substrates on thin film composite membranes: A green solvent approach with TamiSolve® NxG, J. Membr. Sci., 635 (2021) 119530.

[20] S.U. Hong, Y. Wang, L.S. Soh, W.F. Yong, Are green solvents truly green? Integrating life cycle assessment and techno-economic analysis for sustainable membrane fabrication, Green Chem., 25 (2023) 4501-4512.

[21] L. Sing Soh, S. Uyin Hong, C. Zeng Liang, W. Fen Yong, Green solvent-synthesized polyimide membranes for gas separation: Coupling Hansen solubility parameters and synthesis optimization, Chem. Eng. J., 478 (2023) 147451.

[22] F. Galiano, K. Briceño, T. Marino, A. Molino, K.V. Christensen, A. Figoli, Advances in biopolymer-based membrane preparation and applications, J. Membr. Sci., 564 (2018) 562-586.

[23] Y. Zhang, X. Cheng, X. Jiang, J.J. Urban, C.H. Lau, S. Liu, L. Shao, Robust natural nanocomposites realizing unprecedented ultrafast precise molecular separations, Mater. Today, 36 (2020) 40-47.

[24] C. Yang, F. Topuz, S.-H. Park, G. Szekely, Biobased thin-film composite membranes comprising priamine–genipin selective layer on nanofibrous biodegradable polylactic acid support for oil and solvent-resistant nanofiltration, Green Chem., 24 (2022) 5291-5303.

[25] C. Vepari, D.L. Kaplan, Silk as a biomaterial, Prog. Polym. Sci., 32 (2007) 991-1007.

[26] A. Reizabal, C.M. Costa, L. Pérez-Álvarez, J.L. Vilas-Vilela, S. Lanceros-Méndez, Silk Fibroin as Sustainable Advanced Material: Material Properties and Characteristics, Processing, and Applications, Adv. Funct. Mater., 33 (2023) 2210764.

[27] Y. Hu, L. Liu, J. Yu, Z. Wang, Y. Fan, Preparation of Natural Multicompatible Silk Nanofibers by Green Deep Eutectic Solvent Treatment, ACS Sustainable Chem. Eng., 8 (2020) 4499-4510.

[28] W. Xin, Z. Zhang, X. Huang, Y. Hu, T. Zhou, C. Zhu, X.-Y. Kong, L. Jiang, L. Wen, High-performance silk-based hybrid membranes employed for osmotic energy conversion, Nat. Commun., 10 (2019) 3876.

[29] E.L. Smith, A.P. Abbott, K.S. Ryder, Deep Eutectic Solvents (DESs) and Their Applications, Chem. Rev., 114 (2014) 11060-11082.

[30] H.-C. Yang, R.Z. Waldman, M.-B. Wu, J. Hou, L. Chen, S.B. Darling, Z.-K. Xu, Dopamine: Just the Right Medicine for Membranes, Adv. Funct. Mater., 28 (2018) 1705327.

[31] B. Li, Y. Cui, S. Japip, Z. Thong, T.S. Chung, Graphene oxide (GO) laminar membranes for concentrating pharmaceuticals and food additives in organic solvents, Carbon, 130 (2018) 503-514.

[32] X. Tan, W. Zhao, T. Mu, Controllable exfoliation of natural silk fibers into nanofibrils by protein denaturant deep eutectic solvent: nanofibrous strategy for multifunctional membranes, Green Chem., 20 (2018) 3625-3633.

[33] K. Zheng, J. Zhong, Z. Qi, S. Ling, D.L. Kaplan, Isolation of Silk Mesostructures for Electronic and Environmental Applications, Adv. Funct. Mater., 28 (2018) 1806380.

[34] N. Lin, X.Y. Liu, Correlation between hierarchical structure of crystal networks and macroscopic performance of mesoscopic soft materials and engineering principles, Chem. Soc. Rev., 44 (2015) 7881-7915.

[35] L. Xiao, Z. Ding, X. Zhang, X. Wang, Q. Lu, D.L. Kaplan, Silk Nanocarrier Size Optimization for Enhanced Tumor Cell Penetration and Cytotoxicity In Vitro, ACS Biomater. Sci. Eng., 8 (2022) 140-150.

[36] H. Fissan, S. Ristig, H. Kaminski, C. Asbach, M. Epple, Comparison of different characterization methods for nanoparticle dispersions before and after aerosolization, Anal. Methods, 6 (2014) 7324-7334.

[37] F. Zhang, Q. Lu, J. Ming, H. Dou, Z. Liu, B. Zuo, M. Qin, F. Li, D.L. Kaplan, X. Zhang, Silk dissolution and regeneration at the nanofibril scale, J. Mater. Chem. B, 2 (2014) 3879-3885.

[38] C. Guo, J. Zhang, X. Wang, A.T. Nguyen, X.Y. Liu, D.L. Kaplan, Comparative Study of Strain-Dependent Structural Changes of Silkworm Silks: Insight into the Structural Origin of Strain-Stiffening, Small, 13 (2017) 1702266.

[39] Q. Lu, H. Zhu, C. Zhang, F. Zhang, B. Zhang, D.L. Kaplan, Silk Self-Assembly Mechanisms and Control From Thermodynamics to Kinetics, Biomacromolecules, 13 (2012) 826-832.

[40] J. Zhong, M. Ma, W. Li, J. Zhou, Z. Yan, D. He, Self-assembly of regenerated silk fibroin from random coil nanostructures to antiparallel β-sheet nanostructures, Biopolymers, 101 (2014) 1181-1192.

[41] W. Zhao, S. Cao, H. Cai, Y. Wu, Q. Pan, H. Lin, J. Fang, Y. He, H. Deng, Z. Liu, Chitosan/silk fibroin biomimic scaffolds reinforced by cellulose acetate nanofibers for smooth muscle tissue engineering, Carbohydr. Polym., 298 (2022) 120056.

[42] A. Rivera-Galletti, C.R. Gough, F. Kaleem, M. Burch, C. Ratcliffe, P. Lu, D. Salas-de la Cruz, X. Hu, Silk-Cellulose Acetate Biocomposite Materials Regenerated from Ionic Liquid, Polymers, 13 (2021).

[43] M.A. de Moraes, T. Crouzier, M. Rubner, M.M. Beppu, Factors Controlling the Deposition of Silk Fibroin Nanofibrils during Layer-by-Layer Assembly, Biomacromolecules, 16 (2015) 97-104.

[44] H.-F. Xiao, C.-H. Chu, W.-T. Xu, B.-Z. Chen, X.-H. Ju, W. Xing, S.-P. Sun, Amphibian-inspired amino acid ionic liquid functionalized nanofiltration membranes with high water permeability and ion selectivity for pigment wastewater treatment, J. Membr. Sci., 586 (2019) 44-52.

[45] J. Zhu, M. Tian, J. Hou, J. Wang, J. Lin, Y. Zhang, J. Liu, B. Van der Bruggen, Surface zwitterionic functionalized graphene oxide for a novel loose nanofiltration membrane, J. Mater. Chem. A, 4 (2016) 1980-1990.

561